

# On the temperature sensitivity of near-surface seismic wave speeds: application to the Groningen region, the Netherlands

Eldert Fokker<sup>1,2,\*</sup>, Elmer Ruigrok<sup>1,2</sup> and Jeannot Trampert<sup>1</sup>

<sup>1</sup>Department of Earth Sciences, Utrecht University, Princetonlaan 8a, 3584 CB, Utrecht, the Netherlands. E-mail: [eldert.fokker@tmo.nl](mailto:eldert.fokker@tmo.nl)

<sup>2</sup>R&D Seismology and Acoustics, Royal Netherlands Meteorological Institute, Utrechtseweg 297, 3731 GA, De Bilt, the Netherlands

Accepted 2024 March 11. Received 2024 March 4; in original form 2023 September 28

## SUMMARY

Subsurface temperature measurements play a crucial role, for instance, in optimizing geothermal power plants and monitoring heat-storage systems. Previous studies have demonstrated that time-lapse variations in temperature can be correlated with variations in seismic wave speeds, offering the potential for temperature monitoring via seismic surveys. However, an apparent discrepancy has emerged between field and laboratory experiments. Field studies predominantly report positive correlations between temperature and seismic wave speeds, while laboratory experiments often show anticorrelations. This inconsistency underscores the need for a more comprehensive, physics-based understanding of temperature-induced wave speed changes. In this study, we strive to bridge the gap between field and laboratory findings by examining several mechanisms governing temperature-induced seismic wave speed changes, namely the intrinsic temperature dependency of elastic parameters and thermally induced elasticity. We present a physics-based modelling approach to identify the primary mechanisms responsible for temperature-induced seismic wave speed changes. By considering several end-member models, we find that intrinsic temperature dependency of elastic parameters (negative correlation) compete with thermal pressure effects (positive correlation). The precise initial and boundary conditions and physical parameters of the system under consideration will determine the weight of both effects. Temperature-related dilatation does not seem to play an important role. We apply our approach to loosely consolidated sediments in the shallow subsurface of the Groningen region, where subsurface temperature fluctuations are driven by seasonal atmospheric temperature fluctuations roughly between  $-5$  and  $30^{\circ}\text{C}$ . For these models, we predict seasonal temperature-induced changes in body-wave speeds of up to 8 per cent in the first few metres of the subsurface, high-frequency (above 2 Hz) surface wave phase velocity variations in the range of 1–2 per cent, and relative changes in site amplification on the order of 4 per cent. These findings contribute to a more comprehensive understanding of the intricate relationship between temperature and near-surface seismic properties, offering insights for applications as subsurface temperature monitoring systems.

**Key words:** Elasticity and anelasticity; Numerical modelling; Time-series analysis; Surface waves and free oscillations.

## 1 INTRODUCTION

Accurate subsurface temperature measurements are necessary, for instance, for optimizing geothermal power plants and monitoring heat-storage systems. Previous studies showed that time-lapse variations in temperature correlate with variations in seismic wave speeds

(e.g. Richter *et al.* 2014; Lecocq *et al.* 2017; Bièvre *et al.* 2018; Colombero *et al.* 2018; Sleeman & de Zeeuw-van Dalfsen 2020; Ermert *et al.* 2023). This suggests the possibility of using seismic wave speed variations as a means to monitor temperature changes. However, not all mechanisms for temperature-induced wave speed changes have been analysed all at once, and the conditions under which these mechanisms induce measurable seismic wave speed changes are not well understood.

Moreover, field and laboratory studies have yielded seemingly contradictory results when examining the relationship between temperature and seismic wave speed. Most field studies have reported

\* Now at: Department of Hydrology and Reservoir Engineering, TNO Geological Survey of the Netherlands, Princetonlaan 6, 3584 CB, Utrecht, the Netherlands

positive correlations between temperature and seismic wave speed (e.g. Richter *et al.* 2014; Lecocq *et al.* 2017; Sleeman & de Zeeuw-van Dalfsen 2020; Ermert *et al.* 2023), while most laboratory experiments have shown anticorrelations (e.g. Birch 1943; Kohnen 1974; Kern 1978; Christensen 1979; Jaya *et al.* 2010). It is therefore not always clear which mechanisms drive wave speed changes under which conditions.

Understanding the mechanisms behind wave speed changes is therefore important to determine when and where temperature monitoring using seismic signals is feasible. By studying the underlying mechanisms, we can identify the dominant factors contributing to temperature-induced seismic wave speed changes, assess the potential for temperature monitoring using seismic measurements, and infer environmental implications such as the seasonality of site amplifications for instance.

This study first presents a series of physics-based models, identifying temperature-induced changes in seismic properties (Section 2). We then propose an applications in the very shallow subsurface in the Groningen region, The Netherlands, to assess the sensitivity of seismic observables to temperature changes (Section 3). This requires a careful analysis of the initial and boundary conditions and physical properties of the model (Sections 3.1 and 3.2). We then estimate the evolution of subsurface temperatures resulting from forcing by surface temperature diffusion (Section 3.3) and determine the corresponding temperature-induced variations in body-wave speeds and surface wave phase velocities (Section 3.4). Finally, we look at seasonal site amplifications (Section 3.5). We identify the dominant mechanisms driving temperature-induced seismic wave speed changes and find that temperature variations can be monitored using surface-wave phase velocity variations. Interestingly, surface temperature variations can also induce notable changes in site amplifications.

## 2 THEORETICAL BACKGROUND

Seismic wave speed variations are influenced by temperature and pressure changes, assuming the chemistry (including fluids) does not change in the subsurface. Temperature and pressure changes have a direct influence on the elastic parameters, but they also change the elasticity via thermo-elasticity (e.g. Berger 1975) or stress-induced effects (e.g. Tromp & Trampert 2018). Here, we are particularly interested in the two former effects, while later was treated in depth in a different contribution (Fokker *et al.* 2021).

Compressional and shear wave speeds  $v_p$  and  $v_s$  depend on the bulk modulus  $\kappa$ , the shear modulus  $\mu$  and density  $\rho$ :

$$\begin{aligned} v_p &= \sqrt{\frac{\kappa + \frac{4}{3}\mu}{\rho}}, \\ v_s &= \sqrt{\frac{\mu}{\rho}}. \end{aligned} \quad (1)$$

Body-wave speed variations can therefore simply be derived by differentiating eq. (1) to obtain

$$\begin{aligned} \frac{dv_p}{v_p} &= \frac{d\kappa + \frac{4}{3}d\mu}{2(\kappa + \frac{4}{3}\mu)} - \frac{d\rho}{2\rho}, \\ \frac{dv_s}{v_s} &= \frac{d\mu}{2\mu} - \frac{d\rho}{2\rho}. \end{aligned} \quad (2)$$

The bulk and shear modulus are intrinsic functions of temperature  $T$  and pressure  $P$ , hence their differential can be written as

$$\begin{aligned} d\kappa &= \kappa'_T dT + \kappa'_P dP, \\ d\mu &= \mu'_T dT + \mu'_P dP, \end{aligned} \quad (3)$$

with temperature and pressure derivatives of the bulk and shear modulus  $\kappa'_T = (\partial\kappa/\partial T)_P$ ,  $\kappa'_P = (\partial\kappa/\partial P)_T$ ,  $\mu'_T = (\partial\mu/\partial T)_P$  and  $\mu'_P = (\partial\mu/\partial P)_T$ , respectively. From linear elasticity, we know that a relative volume change is given by the dilatation, and again by differentiation, we find that

$$d\epsilon_{kk} = dV/V = -d\rho/\rho, \quad (4)$$

where  $\epsilon_{ij}$  represents components of the strain tensor. By substituting eqs (3) and (4) in eq. (2), we can write the wave speed changes as

$$\begin{aligned} \frac{dv_p}{v_p} &= \frac{\kappa'_T + \frac{4}{3}\mu'_T}{2(\kappa + \frac{4}{3}\mu)} dT + \frac{\kappa'_P + \frac{4}{3}\mu'_P}{2(\kappa + \frac{4}{3}\mu)} dP + \frac{1}{2}d\epsilon_{kk}, \\ \frac{dv_s}{v_s} &= \frac{\mu'_T}{2\mu} dT + \frac{\mu'_P}{2\mu} dP + \frac{1}{2}d\epsilon_{kk}, \end{aligned} \quad (5)$$

where the first terms on the right-hand side represent temperature-induced wave speed changes via the intrinsic temperature dependency of the elastic moduli, the second terms pressure-induced wave speed changes via the intrinsic pressure dependency of elastic moduli and the third terms dilatation changes.

To express the dilatation differential in terms of temperature and pressure variations, we need to consider a constitutive equation relating stress tensor components  $\sigma_{ij}$  to strain tensor components  $\epsilon_{ij}$ . In linearized thermo-elasticity, this relation is given by (e.g. Berger 1975)

$$\sigma_{ij} = \left[ \left( \kappa - \frac{2}{3}\mu \right) \epsilon_{kk} - 3\kappa\alpha_T(T - T_0) \right] \delta_{ij} + 2\mu \epsilon_{ij}, \quad (6)$$

where  $\alpha_T$  represents the coefficient of thermal expansion and  $T_0$  is some reference temperature. The above equation allows us to solve for the dilatation.

$$\epsilon_{kk} = 3\alpha_T(T - T_0) + \frac{\sigma_{kk}}{3\kappa}. \quad (7)$$

Differentiating, reusing eq. (3) and realizing that  $\sigma_{kk} = -3P$ ,

$$d\epsilon_{kk} = 3\alpha_T dT - \frac{dP}{\kappa} + \frac{P\kappa'_T dT}{\kappa^2} + \frac{P\kappa'_P dP}{\kappa^2}. \quad (8)$$

This last equation allows us to investigate the different terms contributing to the density perturbations in eq. (2) in more detail. With seismology we are often able to measure wave speed variations of the order of a tenth of a percent.  $\alpha_T$  is of the order  $10^{-6}$ – $10^{-5} \text{ } ^\circ\text{C}^{-1}$ , unless the temperature variation is hundreds to thousands of degrees, the first term can be neglected for the shallow subsurface and even the entire crust.  $\kappa$  is of the order  $10^9 \text{ Pa}$ , unless the pressure variation is of the order of MPa, the second term can also be neglected. The next two terms are elasticity contributions, which for the shallow subsurface, where  $P$  is of the order of kPa, are also too small to contribute. We can thus conclude that  $d\epsilon_{kk} \approx 0$  for most situations in the shallow subsurface. This leaves us only with contributions from temperature and pressure derivatives of the elastic moduli in eq. (5).

These are general considerations, and we have so far neither considered initial conditions (reference  $T$ ,  $P$ ,  $\kappa$ ,  $\mu$  and  $\rho$ ) nor boundary conditions for any specific medium. Considering some end-member media gives us insight into what to expect.

Let us first consider a medium which is free to expand, meaning that all stress components are zero at all time, and as a consequence

the medium cannot sustain any pressure changes ( $dP = 0$ ). From eq. (7), we further see that  $\epsilon_{kk} = 3\alpha_T(T - T_0)$  and hence  $d\epsilon_{kk} = 3\alpha_T dT$ . Finally, we arrive at

$$\begin{aligned}\frac{dv_p}{v_p} &= \frac{\kappa'_T + \frac{4}{3}\mu'_T}{2(\kappa + \frac{4}{3}\mu)} dT + \frac{3}{2}\alpha_T dT, \\ \frac{dv_s}{v_s} &= \frac{\mu'_T}{2\mu} dT + \frac{3}{2}\alpha_T dT.\end{aligned}\quad (9)$$

For parameters we can reasonably expect to occur in the subsurface, we note that the first term dominates over  $\alpha_T dT$  and the temperature changes should correlate negatively with velocity changes as predicted by mineral physics measurements.

Another end-member medium is one where the expansion is totally restricted, meaning that all strain components remain zero at all time. This results in  $\sigma_{kk} = -3P = -9\alpha_T \kappa(T - T_0)$ , or  $dP = 3\alpha_T \kappa dT$ . We then arrive at the following velocity perturbations

$$\begin{aligned}\frac{dv_p}{v_p} &= \frac{\kappa'_T + \frac{4}{3}\mu'_T}{2(\kappa + \frac{4}{3}\mu)} dT + \frac{\kappa'_p + \frac{4}{3}\mu'_p}{2(\kappa + \frac{4}{3}\mu)} 3\alpha_T \kappa dT, \\ \frac{dv_s}{v_s} &= \frac{\mu'_T}{2\mu} dT + \frac{\mu'_p}{2\mu} 3\alpha_T \kappa dT.\end{aligned}\quad (10)$$

For parameters we can reasonably expect to occur in the subsurface, we note that now the second terms on the right-hand side dominate (because  $\kappa$  is large), which is nothing else but terms due to thermal pressure at constant volume, and the temperature changes should correlate positively with velocity changes.

We thus note that mineral physics conditions or thermal pressure compete for negative or positive wave speed correlations and the precise boundary conditions and elastic parameters active in the medium determine their respective weight.

A last end-member case of interest is one of simple elasticity where  $T = T_0$  strictly at all time and thermal expansion does not play a role. This case was treated in detail in Fokker *et al.* (2021) and reduces to

$$\begin{aligned}\frac{dv_p}{v_p} &= \frac{\kappa'_p + \frac{4}{3}\mu'_p}{2(\kappa + \frac{4}{3}\mu)} dP, \\ \frac{dv_s}{v_s} &= \frac{\mu'_p}{2\mu} dP,\end{aligned}\quad (11)$$

where we interpreted  $dP = -du$  as change in effective pressure, due to pore pressure change  $du$ .

Above we established how wave speeds change with temperature and pressure. Most subsurface seismic monitoring relies on seismic interferometry (e.g. Sens-Schönfelder & Wegler 2006), which often provides information on surface wave dispersion. Surface wave phase velocity changes are mainly caused by changes in shear wave velocities. For small velocity changes this can then be written as

$$\frac{dc_R}{c_R}(\omega) = \int_0^\infty (K_s^R(\omega, z) d \ln v_s(z)) dz, \quad (12)$$

$$\frac{dc_L}{c_L}(\omega) = \int_0^\infty (K_s^L(\omega, z) d \ln v_s(z)) dz, \quad (13)$$

where  $c_R$  and  $c_L$  represent Rayleigh- and Love-wave phase velocities as a function of angular frequency  $\omega$ , and shear wave sensitivity kernels are indicated by  $K_s^R$  and  $K_s^L$  for Rayleigh and Love waves, respectively. Since the shear wave speeds depends on temperature, we can define surface wave temperature sensitivities as

$$K_T^{R,L}(\omega, z) = K_s^{R,L}(\omega, z) \frac{d \ln v_s}{dT}(z). \quad (14)$$

### 3 TEMPERATURE-INDUCED VARIATIONS IN SEISMIC PROPERTIES: CASE OF THE GRONINGEN SUBSURFACE

Based on the theoretical framework of the previous section, we now attempt to characterize temperature-induced variations in seismic wave speeds and site amplification. Physics-based modelling requires knowledge of a long list of parameters that are not often available. We have chosen a location where many observations are present: the Groningen subsurface of the Netherlands. Section 3.1 describes the specific initial and boundary conditions for our chosen region of study and explains how, under these specific conditions, subsurface temperature variations may affect seismic wave speeds. Section 3.2 describes the relevant physical parameters for the modelling exercise. In Section 3.3, we describe a potential forcing of subsurface temperature variations via heat diffusion. This allows us to estimate the temperature sensitivity of seismic waves (Section 3.4) given the initial and boundary conditions, the medium parameters and the surface temperature forcing. A last, but interesting, application is how temperature variations affect site amplification. (Section 3.5). The latter is useful for seismic hazard assessment in the region.

#### 3.1 Initial and boundary conditions and effects on seismic wave speeds

To precisely assess all the terms in eq. (5), we need to specify initial and boundary conditions for the medium under consideration.

First, we choose the initial stress state to be hydrostatic pressure,

$$\sigma_{ij}(z) = -P(z)\delta_{ij} = -\int_0^z \rho(z')g dz' \delta_{ij}, \quad (15)$$

with density  $\rho$ , gravitational acceleration  $g$  and depth  $z$ . Further assuming that the initial temperature is equal to the reference temperature ( $T = T_0$ ), eq. (6) leads to initial strain

$$\epsilon_{ij} = -\frac{1}{3\kappa} P \delta_{ij}, \quad (16)$$

and these initial conditions allow us to express the differential of eq. (6) as

$$d\sigma_{ij} = 2\mu d\epsilon_{ij} + \left( -\frac{d\kappa}{\kappa} P + \left( \kappa - \frac{2}{3}\mu \right) d\epsilon_{kk} - 3\kappa\alpha_T dT \right) \delta_{ij}. \quad (17)$$

Next we have to specify boundary conditions. In a horizontally infinite medium, or a medium with rigid boundaries, there is no horizontal strain. As this applies to our region of interest, we assume horizontal strains to be static:

$$d\epsilon_{xx} = d\epsilon_{yy} = 0. \quad (18)$$

In the vertical direction, however, the material is free to expand, naturally restricting changes in vertical stress:

$$d\sigma_{zz} = 0. \quad (19)$$

Applying these boundary conditions to eq. (17), while writing out all diagonal components, leads to the following expressions:

$$\begin{aligned}d\sigma_{xx} = d\sigma_{yy} &= -\frac{d\kappa}{\kappa} P + \left( \kappa - \frac{2}{3}\mu \right) d\epsilon_{zz} - 3\kappa\alpha_T dT, \\ 0 &= -\frac{d\kappa}{\kappa} P + \left( \kappa + \frac{4}{3}\mu \right) d\epsilon_{zz} - 3\kappa\alpha_T dT.\end{aligned}\quad (20)$$

Since the bulk modulus is a function of temperature and pressure (eq. 3), and the pressure differential is

$$dp = -\frac{d\sigma_{xx} + d\sigma_{yy}}{3}, \quad (21)$$

we now have enough information to deduce temperature-induced changes in pressure and dilation.

To obtain the relevant expressions, we form a system of equations consisting of eqs (3), (20) and (21), and solve for  $dp$  and  $d\epsilon_{kk}$ :

$$dp = \frac{4\mu(P\kappa'_T + 3\kappa^2\alpha_T)}{3\kappa^2 + 4\kappa\mu - 4\mu\kappa'_P P} dT, \quad (22)$$

$$d\epsilon_{kk} = d\epsilon_{zz} = \frac{3(P\kappa'_T + 3\kappa^2\alpha_T)}{3\kappa^2 + 4\kappa\mu - 4\mu\kappa'_P P} dT. \quad (23)$$

Replacing in eq. (5), we obtain the changes in wave speeds due to temperature as

$$d \ln v_p = \frac{dv_p}{v_p} = \frac{\kappa'_T + \frac{4}{3}\mu'_T}{2(\kappa + \frac{4}{3}\mu)} dT + \frac{\kappa'_P + \frac{4}{3}\mu'_P}{2(\kappa + \frac{4}{3}\mu)} \frac{4\mu(P\kappa'_T + 3\kappa^2\alpha_T)}{3\kappa^2 + 4\kappa\mu - 4\mu\kappa'_P P} dT + \frac{1}{2} \frac{3(P\kappa'_T + 3\kappa^2\alpha_T)}{3\kappa^2 + 4\kappa\mu - 4\mu\kappa'_P P} dT, \quad (24)$$

$$d \ln v_s = \frac{dv_s}{v_s} = \frac{\mu'_T}{2\mu} dT + \frac{\mu'_P}{2\mu} \frac{4\mu(P\kappa'_T + 3\kappa^2\alpha_T)}{3\kappa^2 + 4\kappa\mu - 4\mu\kappa'_P P} dT + \frac{1}{2} \frac{3(P\kappa'_T + 3\kappa^2\alpha_T)}{3\kappa^2 + 4\kappa\mu - 4\mu\kappa'_P P} dT. \quad (25)$$

All parameters of eqs (24) and (25) are a function of depth  $z$ . Dividing by  $dT$  leads to the temperature sensitivity of body-wave speeds (i.e. the relative change in velocity due to a change in temperature).

### 3.2 Physical properties of the model

Physics-based modelling of temperature-induced variations in seismic wave speeds requires models correctly describing the physical properties. We use models from the subsurface of the province of Groningen in the Netherlands, and lab experiments on similar (semi-)unconsolidated materials. The Groningen region provides an ideal setting for physics-based modelling due to its well-documented geological and geophysical characteristics. Moreover, we can rely on air temperature measurements from the meteorological station in Eelde, operated by the Royal Netherlands Meteorological Institute (KNMI 2023). Table 1 shows a list of all the properties and mathematical definitions used in this study.

We gather shear wave velocity and density models from Ntinalexis *et al.* (2023) and a compressional-wave velocity model from Romijn (2017), all at the location of seismic station G08 (KNMI 1993). From these models, we can compute all elastic parameters needed for this study. Following Fokker *et al.* (2021, 2023), we compute the pressure derivative of the bulk and shear moduli by a pointwise derivative of the bulk and shear moduli with respect to the confining pressure. A smoothing operation with a robust weighting function and positivity constraint removes outliers that occur at layer intersections. Figs 1(a)–(h) show the elastic models used in this study. The detailed models of Ntinalexis *et al.* (2023) in blue have been smoothed for this study to obtain the black curves. For this smoothing process, we applied local regression using a weighted linear least squares and a first degree polynomial model.

Thermo-elastic model parameters should be selected from experiments on similar unconsolidated materials. Temperature derivatives of the bulk and shear moduli can only be determined in a laboratory setting. For fully saturated clay, Bentil & Zhou (2022) found that

**Table 1.** Definitions used in this study, organized by the Roman and Greek alphabet.

$c_L$	Love-wave phase velocity [m s <sup>-1</sup> ]
$c_R$	Rayleigh-wave phase velocity [m s <sup>-1</sup> ]
$d \ln v$	Alternative notation for relative velocity change: $d \ln v = \frac{dv}{v}$
$F_p$	Amplification factor for compressional waves [–]
$F_s$	Amplification factor for shear waves [–]
$K_s^L$	Shear wave velocity sensitivity kernel for Love-wave phase velocity [m <sup>-1</sup> ]
$K_s^R$	Shear wave velocity sensitivity kernel for Rayleigh-wave phase velocity [m <sup>-1</sup> ]
$K_T^L$	Temperature sensitivity kernel for Love-wave phase velocity [°C <sup>-1</sup> m <sup>-1</sup> ]
$K_T^R$	Temperature sensitivity kernel for Rayleigh-wave phase velocity [°C <sup>-1</sup> m <sup>-1</sup> ]
$P$	Pressure [Pa]
$t$	Time [s]
$T$	Temperature [°C]
$u$	Pore pressure [Pa]
$v$	Seismic velocity [m s <sup>-1</sup> ]
$v_p$	Compressional-wave velocity [m s <sup>-1</sup> ]
$v_s$	Shear wave velocity [m s <sup>-1</sup> ]
$z$	Depth [m]
$\alpha_d$	Thermal diffusivity [m <sup>2</sup> s <sup>-1</sup> ]
$\alpha_T$	Thermal expansion coefficient [°C <sup>-1</sup> ]
$\delta_{ij}$	Kronecker delta, yielding 1 for $i = j$ and 0 otherwise
$\epsilon_{ij}$	Strain tensor [–], defined positive for increased volume
$\kappa$	Bulk modulus [Pa]
$\kappa'_P$	Pressure derivative of the bulk modulus [–]
$\kappa'_T$	Temperature derivative of the bulk modulus [Pa °C <sup>-1</sup> ]
$\mu$	Shear modulus [Pa]
$\mu'_P$	Pressure derivative of the shear modulus [–]
$\mu'_T$	Temperature derivative of the shear modulus [Pa °C <sup>-1</sup> ]
$\rho$	Mass density [kg m <sup>-3</sup> ]
$\sigma_{ij}$	Stress tensor [Pa], defined negative for compression
$\omega$	Angular frequency [rad s <sup>-1</sup> ]

after multiple thermal cycles the temperature derivative of the shear modulus is in the order of  $\mu'_T \sim -0.6 \cdot 10^6$  Pa °C<sup>-1</sup> (Fig. 1i). For the temperature derivative of the bulk modulus, however, we could not find values for unconsolidated materials. At a temperature of  $T = 20^\circ\text{C}$ , values are reported to be  $\kappa'_T = -5.3 \times 10^6$  and  $-18 \times 10^6$  Pa °C<sup>-1</sup> for quartz and calcite, respectively (Dandekar & Ruoff 1968; Ohno 1995; Lakshtanov *et al.* 2007; Orlander *et al.* 2021). In this study, we use the value for quartz (Fig. 1j), although this might be a slight overestimation for unconsolidated materials.

Thermal expansion coefficients can be as small as  $\alpha_T \sim 10 \times 10^{-6}$  °C<sup>-1</sup> (Svidró *et al.* 2020; Radkovský *et al.* 2022), whereas for natural clays and sands we find values from  $\alpha_T \sim 18 \times 10^{-6}$  to  $\sim 22 \times 10^{-6}$  °C<sup>-1</sup> (McKinstry 1965; Bobrowski *et al.* 2018). For the purpose of this study, we use  $\alpha_T = 20 \times 10^{-6}$  °C<sup>-1</sup>, independent of depth (Fig. 1k). As thermal diffusivity of clayey sands, Kooi (2008) reported a value of  $\alpha_d = 2.2 \times 10^{-6}$  m<sup>2</sup> s<sup>-1</sup>, which we adopt in our study, independent of depth (Fig. 1l).

### 3.3 Temperature forcing in the Groningen subsurface by heat diffusion modelling

Subsurface temperature variations can be computed with a finite-difference method using surface temperature measurements and the thermal diffusivity (e.g. Pham 1985). We assume here that temperature predominantly varies with time and vertical direction. In this case, heat transport through diffusion can be described by the 1-D

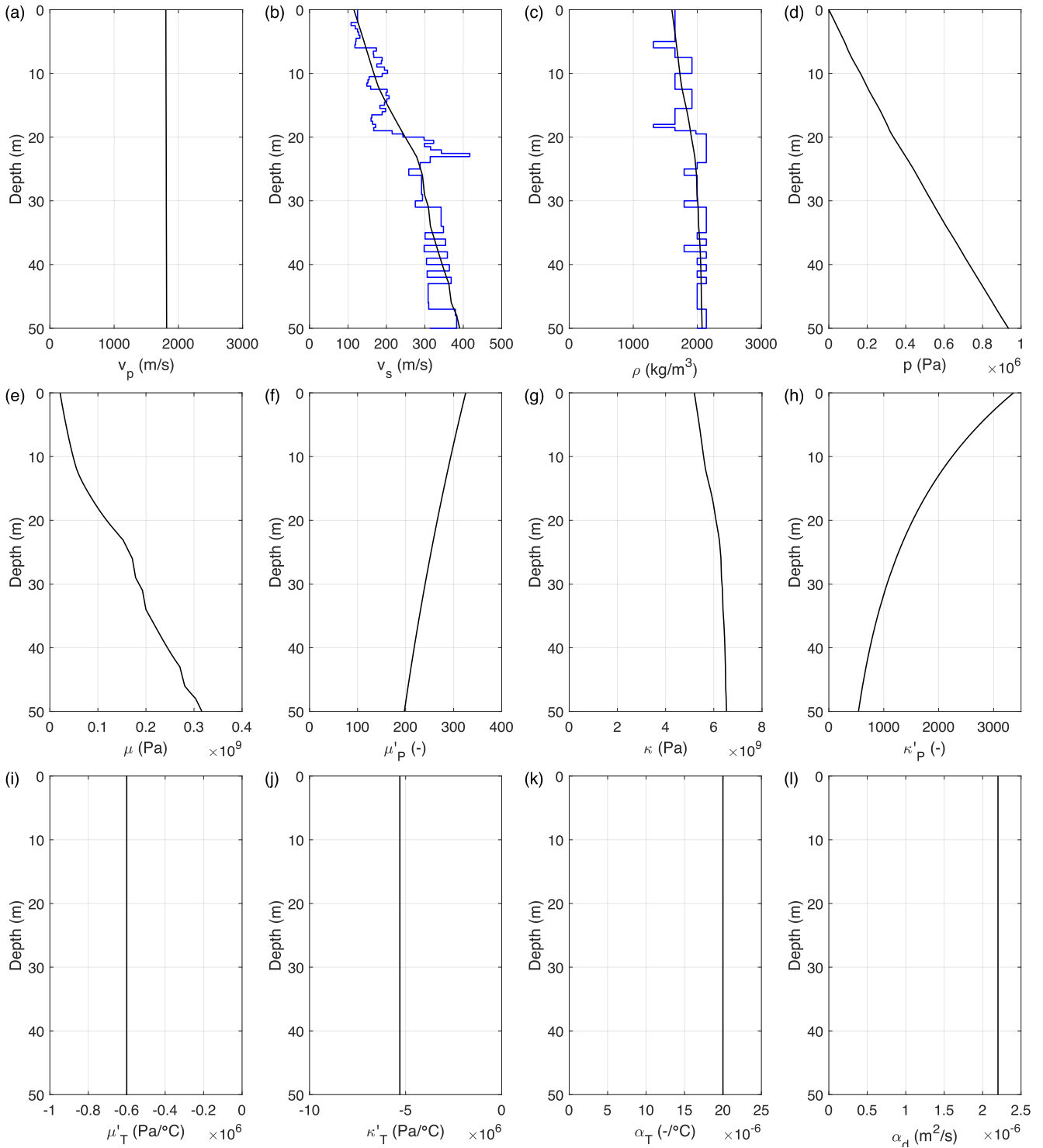


**Figure 1.** Models of physical properties used in this study, as a function of depth: (a) compressional-wave velocity  $v_p$  retrieved from Romijn (2017), (b) shear wave velocity  $v_s$  from Ntinalexis *et al.* (2023) in blue and smoothed in black, (c) mass density  $\rho$  as presented by Ntinalexis *et al.* (2023) in blue and smoothed in black, (d) confining pressure under hydrostatic condition,  $p(z) = \int_0^z \rho(z')g dz'$ , (e) smoothed shear modulus  $\mu = \rho v_s^2$ , (f) smoothed derivative of the shear modulus with respect to the confining pressure  $\mu'_p = \partial\mu/\partial p$ , (g) smoothed bulk modulus  $\kappa = \rho v_p^2 - \frac{4}{3}\rho v_s^2$ , (h) smoothed derivative of the bulk modulus with respect to the confining pressure  $\kappa'_p = \partial\kappa/\partial p$ , (i) temperature derivative of the shear modulus  $\mu'_T = \partial\mu/\partial T$  for saturated clay after multiple thermal cycles (Bentil & Zhou 2022), (j) temperature derivative of the bulk modulus  $\kappa'_T = \partial\kappa/\partial T$  for quartz (Ohno 1995; Lakshtanov *et al.* 2007; Orlander *et al.* 2021), (k) estimate of the thermal expansion coefficient  $\alpha_T$  for unconsolidated materials (McKinstry 1965; Bobrowski *et al.* 2018) and (l) thermal diffusivity  $\alpha_d$  for clayey sands as reported by Kooi (2008).



heat diffusion equation,

$$\frac{\partial T}{\partial t}(z, t) = \alpha_d(z) \frac{\partial^2 T}{\partial z^2}(z, t), \quad (26)$$

where  $\alpha_d$  represents the thermal diffusivity of the medium, and  $\partial T/\partial t$  describes the change in temperature over time and  $\partial^2 T/\partial z^2$  represents the 1-D Laplacian of temperature  $T$ . Knowing the surface temperature evolution, that is, air temperature measurements in Eelde (KNMI 2023), and the thermal diffusivity ( $\alpha_d \sim 2.2 \times 10^{-6} \text{ m}^2 \text{ s}^{-1}$ ; Kooi 2008), we model the subsurface temperature evolution by (1) updating the temperature model at the surface using the air temperature measurements at time  $t = \tau$ ,

$$T(z = 0, t = \tau) = T^{(\text{air})}(t = \tau), \quad (27)$$

(2) computing temperature change over time-step  $\Delta t$ ,

$$\Delta T(z_i, t = \tau) = \alpha_d(z_i) \frac{\partial^2 T}{\partial z^2}(z_i, t = \tau) \Delta t, \quad (28)$$

using the second discrete space derivative

$$\frac{\partial^2 T}{\partial z^2}(z_i) = \frac{T(z_{i+1}) - 2T(z_i) + T(z_{i-1}))}{\Delta z^2}, \quad (29)$$

and (3) updating the temperature model for the next time-step  $t = \tau + \Delta t$ ,

$$T(z_i, t = \tau + \Delta t) = T(z_i, t = \tau) + \Delta T(z_i, t = \tau). \quad (30)$$

We start from a uniform temperature model, fixed at the average air temperature over six years  $T_{\text{avg}}^{(\text{air})} = 10.4^\circ \text{C}$ , and repeat steps (1), (2) and (3) for time-steps of  $\Delta t = 600 \text{ s}$  and vertical steps of  $\Delta z = 0.1 \text{ m}$  to obtain a temperature model as a function of depth and time. The results are shown in Fig. 2, revealing a generic diffusion behaviour: a thermal wave with a rapid decrease in temperature variations with depth and a time delay increasing with depth (e.g. Mandelis 2001). At 10 m depth, we find a time delay of approximately four months with respect to the surface temperature and temperature differences between summer and winter are in the order of  $1.5^\circ \text{C}$ . Daily temperature variations do not penetrate further than 1 m into the subsurface. The results of Fig. 2 are in the same order of magnitude as the direct subsurface temperature measurements by Bense & Kooi (2004, fig. 3) and Kole *et al.* (2020, fig. 29) with distributed temperature sensing at a similar site in Groningen. The temperature variations presented here will be used to drive  $dT$  in the following sections.

### 3.4 Temperature sensitivities of seismic waves

Using eqs (22) and (23) divided by  $dT$ , for the elastic and the thermo-elastic models presented in Section 3.2, we compute the temperature sensitivity of pressure and strain. Fig. 3 shows the temperature sensitivity for pressure (a) and volumetric strain (b) as a function of depth. For Fig. 3(a), the steep increase of the sensitivity with depth can be explained by the rapid increase in shear modulus  $\mu$ . The sensitivity of the dilation is positive but small. This directly implies that density will decrease when temperatures increases, but the numbers are small, so the effect will be negligible as we already conjectured in Section 2.

Using the solutions in eqs (24) and (25) divided by  $dT$ , for the elastic and the thermo-elastic models presented in Section 3.2, we compute the temperature sensitivity of compressional- and shear wave velocities. Fig. 3 shows the temperature sensitivity of  $v_p$  (c) and  $v_s$  (d) as a function of depth, for each mechanism separately (red, orange and blue) and for their sum (black).

Figs 3(c) and (d) clearly show the opposing signs of the different mechanisms. Velocity changes via the intrinsic temperature dependency of the elastic parameters (red) are negatively affected by temperature, since the temperature derivatives of the bulk and shear moduli are negative. Velocity changes through thermal pressure (orange) and density (blue), on the other hand, are positively affected by temperature, since  $|p\kappa'_T| < 3\kappa^2\alpha_T$  and all other parameters are positive. The contribution from dilatation shows velocity changes two orders of magnitude smaller, hence this mechanism can be neglected as discussed above. Although the two dominant mechanisms have clearly opposing effects on the velocities, the amplitudes of velocity change through thermal pressure and the intrinsic temperature dependency of elastic constants are of the same order of magnitude. Therefore, the total effect can be positive or negative, depending on the physical parameters and conditions. For the Groningen subsurface, we note total velocity changes with a negative sign from 0 to 6 m depth, and a positive sign beyond 6 m depth.

Knowing the temperature sensitivity of compressional and shear wave speeds, we can now model wave speed variations due to a forcing by surface temperature variations as modelled in Section 3.3. Temperature changes  $dT(t, z)$  are constructed from the temperature model presented in Fig. 2 by removing the mean temperature over six years, and substituted in eqs (24) and (25). Fig. 4 shows the modelled velocity variations as a function of time and depth for compressional waves (a) and (b) and shear waves (c) and (d). The distinct change in sign at a depth of 6 m can again be explained by the transition from one dominant mechanism to another. Velocity changes in the first 6 m are dominated by the intrinsic temperature dependencies of the bulk and the shear moduli, while below a depth of 6 m velocity changes are dominated by thermally induced pressure.

To obtain temperature sensitivity kernels for Rayleigh and Love waves, we compute shear wave sensitivity kernels  $K_s^R$  and  $K_s^L$  using the adjoint method (Hawkins 2018) on the 1-D profiles for compressional-wave velocity, shear wave velocity and density presented in Section 3.2, and multiply them with the temperature sensitivity of the shear wave velocity  $\ln v_s/dT$  as displayed by the black curve in Fig. 3(d). Fig. 5 shows temperature sensitivity kernels for Rayleigh (a) and Love (b) waves. We find again a distinct sign change at 6 m depth, corresponding to the sign change in Fig. 3(d).

Phase-velocity changes of Rayleigh and Love waves are then modelled using eqs (12) and (13), the temperature sensitivity kernels shown in Fig. 5, and the temperature variations as modelled in Section 3.3. Fig. 6 shows the Rayleigh and Love wave velocity changes as a function of time and frequency. Unlike Figs 3(c) and (d), 4 and 5, Fig. 6 does not show the distinct sign change associated with a change in mechanism. This can be explained by the amplitude decay with depth of the temperature variations. This leads to very small changes in low-frequency surface-wave phase velocity. Velocity changes of Love waves can be neglected below 2 Hz, while for Rayleigh-wave velocity change can be neglected below 4 Hz. Besides the differences frequency-wise, velocity changes of Love waves are also larger in amplitudes compared to Rayleigh waves. This can be explained by the shallower sensitivity of Love-wave velocities in general.

### 3.5 Site amplification

Amplifications of relatively small earthquake motions in the Groningen region have led to considerable damage (Bommer *et al.* 2017; Kruiver *et al.* 2017; Rodriguez-Marek *et al.* 2017; van Ginkel *et al.* 2019). Shallow soft sedimentary layers overlaying harder

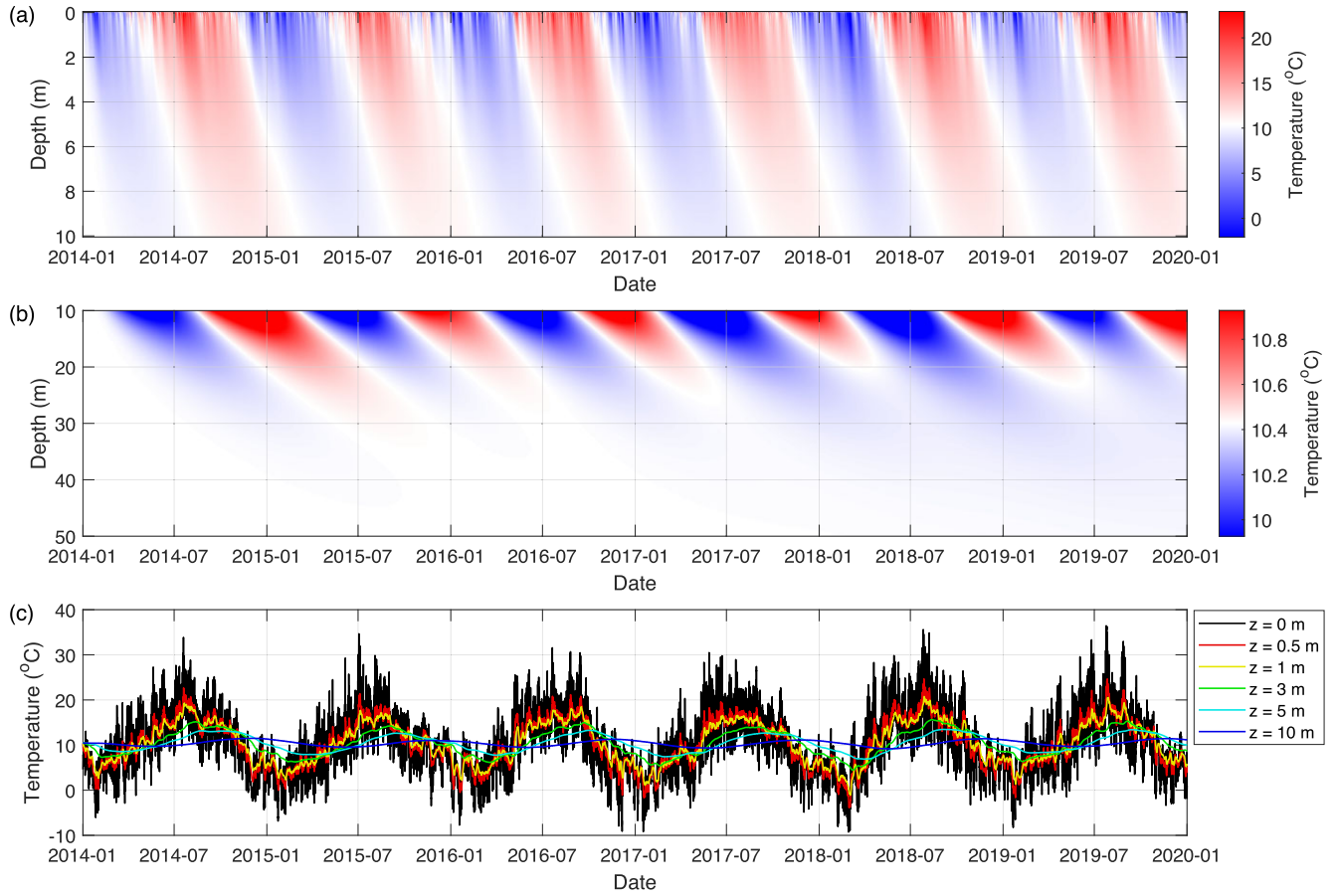


**Figure 2.** Temperature diffusion model for clayey sands ( $\alpha_d = 2.2 \times 10^{-6} \text{ m}^2 \text{ s}^{-1}$ ; Kooi 2008) as a function of time and depth in different visualizations: (a) colour plot for the depth range 0–10 m, (b) colour plot clipped at temperature range 9.9–10.9 °C for the depth range 10–50 m and (c) line plots for various depth levels. Yearly temperature variations are clearly shown in all visualizations, whereas the daily variations are only visible in (a) and (c).

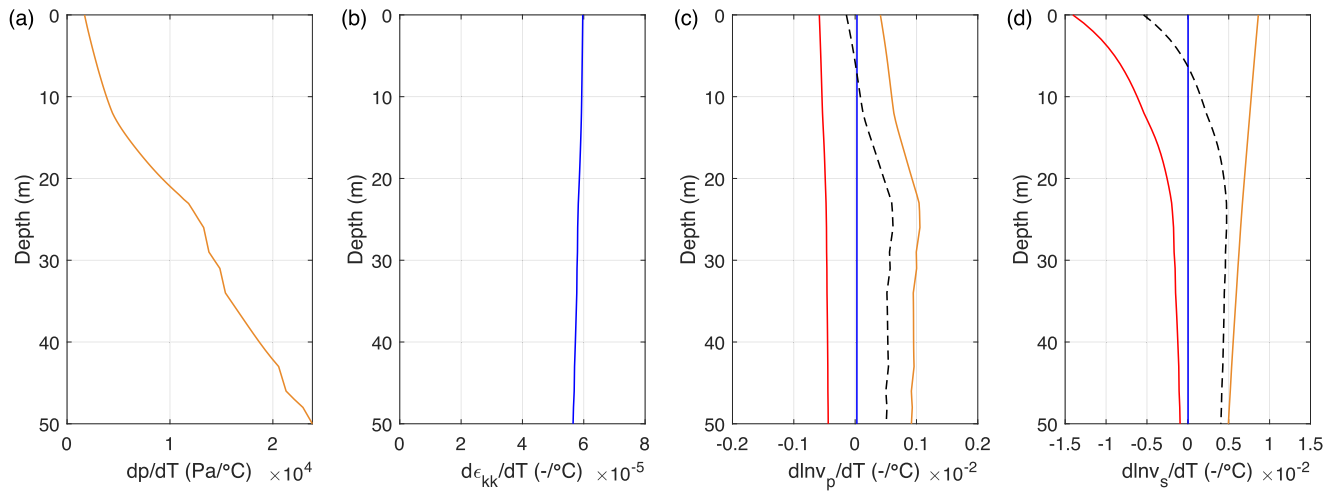


**Figure 3.** Sensitivities to temperature changes as functions of depth for the elastic and the thermo-elastic models presented in Section 3.2. Temperature sensitivity of pressure (a) and volumetric strain (b) in accordance with eqs (22) and (23), respectively. Sensitivity of compressional- (c) and shear wave velocities (d) to temperature variations in accordance with eqs (24) and (25) for three mechanisms separately and for their sum. The red curves indicate the temperature sensitivities via the intrinsic temperature dependency of the elastic parameters, the orange curves show sensitivities through thermally induced pressure, the blue curves reveal the sensitivity through thermally induced strain and the black dashed curves show the sum of all mechanism in accordance with eqs (24) and (25).

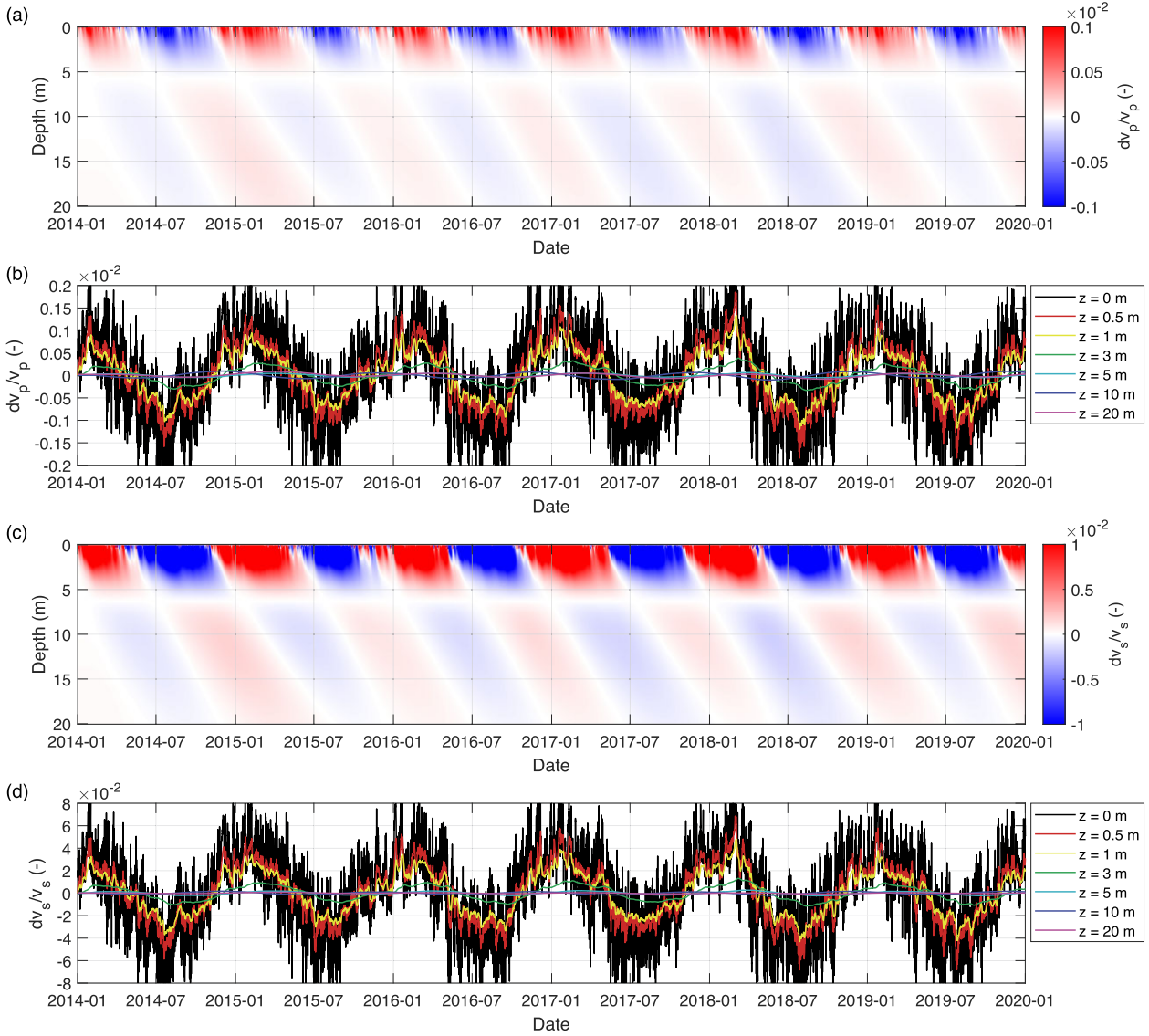


**Figure 4.** Variations in body-wave velocities due to the temperature variations modelled in Section 3.3 (Fig. 2), visualized here as a function of time and depth. Velocity variations of compressional waves (a) and (b) and shear waves (c) and (d) are plotted as colour plots (a) and (c) and line plots (b) and (d). The models of velocity change were obtained by a multiplication of the temperature model presented in Fig. 2, reduced by the mean temperature over six years, and the temperature sensitivities of compressional- and shear wave velocities as displayed in Figs 3(c) and (d).

bedrock are known to amplify ground motion generated by earthquakes: ground motions are amplified by the low impedance (density times velocity) of the shallow layers (Bard *et al.* 1988; Bradley 2012). As the impedance contrast determines the amplification factor, velocity variations in shallow layers contribute directly to changes in site amplification. Here, we derive how the relative changes in compressional- and shear wave velocity affect site amplification.

Ruigrok *et al.* (2022, appendix A) compared two approaches to compute the amplification factor using density and velocity, either using the Zoeppritz equation at every single interface, or assuming a smooth impedance gradient. The difference between the two approaches decreases with an increasing number of layers.

For smooth impedance gradients, the amplification term can be written as

$$F(z_1, z_2) = \sqrt{\frac{\rho_2 v_2}{\rho_1 v_1}}, \quad (31)$$

with  $\rho_1$  and  $v_1$  density and velocity corresponding to depth  $z_1$ , and  $\rho_2$  and  $v_2$  density and velocity corresponding to depth  $z_2$ . The amplification factor describes the relative increase in signal amplitude, when travelling from depth  $z_2$  up to  $z_1$ . A temperature-induced change in velocity at depth  $z_1$ , while depth  $z_2$  is not subjected to change (because our temperature forcing does not diffuse deep enough), leads to a relative change in amplification of

$$\frac{dF}{F}(z_1) = -\frac{1}{2} \frac{dv_1}{v_1}, \quad (32)$$

with  $dv_1/v_1$  the relative velocity change at depth  $z_1$ . Hence, a velocity increase leads to a decrease in amplification with half the amplitude.

Temperature-induced changes in amplification are computed using eq. (32) for compressional- and shear wave velocity change at the surface (i.e.  $z = 0$  m) as computed in Section 3.4 (Fig. 4). Fig. 7 shows the amplification factors due to temperature-induced changes in body-wave velocity at the surface. The amplification factor for



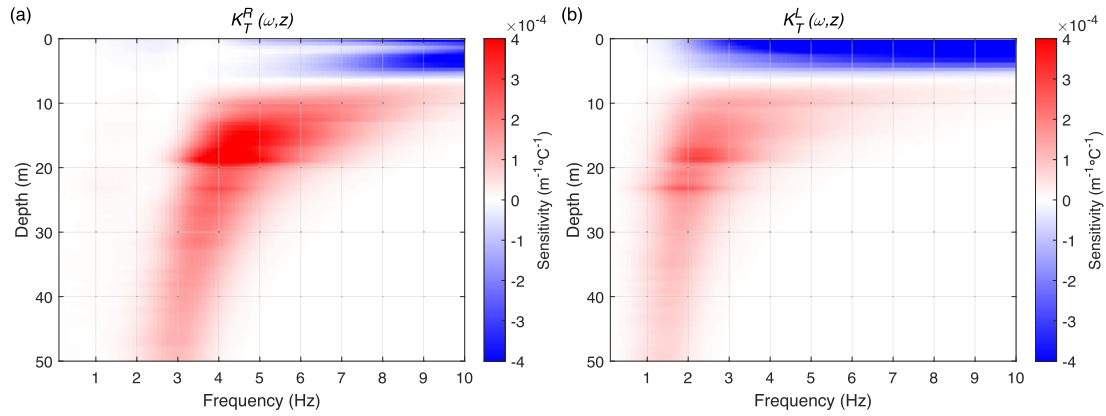


**Figure 5.** Temperature sensitivity kernels for Rayleigh (a) and Love waves (b), as computed using eq. (14). Shear wave sensitivity kernels  $K_s^R$  and  $K_s^L$  have been computed using the adjoint method (Hawkins 2018) on the elastic parameters presented in Section 3.2, and multiplied by the temperature sensitivities of the shear wave velocity (eq. 25; Fig. 3d).

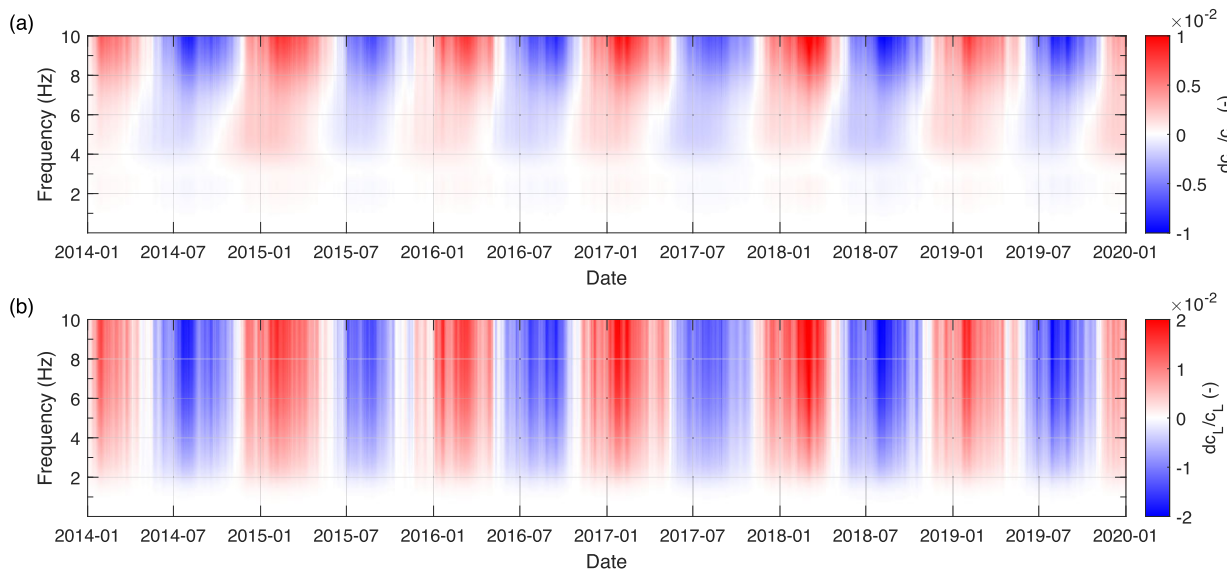


**Figure 6.** Variations in surface-wave phase velocities due to the temperature variations modelled in Section 3.3 (Fig. 2), visualized here as a function of time and frequency. Velocity variations of Rayleigh waves (a) and Love waves (b) are plotted as colour plots. The models of velocity change were computed in accordance with (a) eq. (12) and (b) eq. (13) for the temperature model presented in Fig. 2, reduced by the mean temperature over six years, and the temperature sensitivity kernels for Rayleigh- and Love-wave velocities as displayed in Figs 5(a) and (b).

compressional waves changes by  $dF_p/F_p \sim 0.1$  per cent from winter to summer, while for shear waves we find values of  $dF_s/F_s \sim 4$  per cent from winter to summer.

#### 4 DISCUSSION

In this study, we delved into the physics of seismic wave speed changes caused by temperature variations. We established relationships based on fundamental principles. However, it is important to note that we did not account for all possible factors in our analysis (we neglected chemical and fluids changes for instance), and therefore, our models may not fully account for all the observations found in the existing literature. Nonetheless, for (semi-)unconsolidated materials, we are confident that our investigation captures the dominant mechanisms for temperature-induced seismic wave speed changes.

In Section 3.2, we selected physical parameters for the shallow subsurface of Groningen or for similar unconsolidated materials from existing literature. However, the current studies lack readily available temperature derivatives for bulk and shear moduli. For unconsolidated materials, we came across only one study that explores the connection between the shear modulus and temperature (Bentil & Zhou 2022), and none that investigates the temperature dependency of the bulk modulus. For the latter, we therefore resorted to values determined for quartz (Ohno 1995; Lakshtanov *et al.* 2007; Orlander *et al.* 2021), which may be an overestimation. Less negative values for  $\kappa'_T$  would, in accordance with eqs (24) and (25), shift the red curve in Fig. 3(c) (intrinsic temperature dependency) towards less negative values, while the orange curves in Figs 3(c) and (d) would shift to slightly more positive values. Halving the value of  $\kappa'_T$  just pushes compressional wave speed changes to the positive regime (Fig. 3c, black), while shear wave speed changes remain mostly unaffected. As an alternative to laboratory

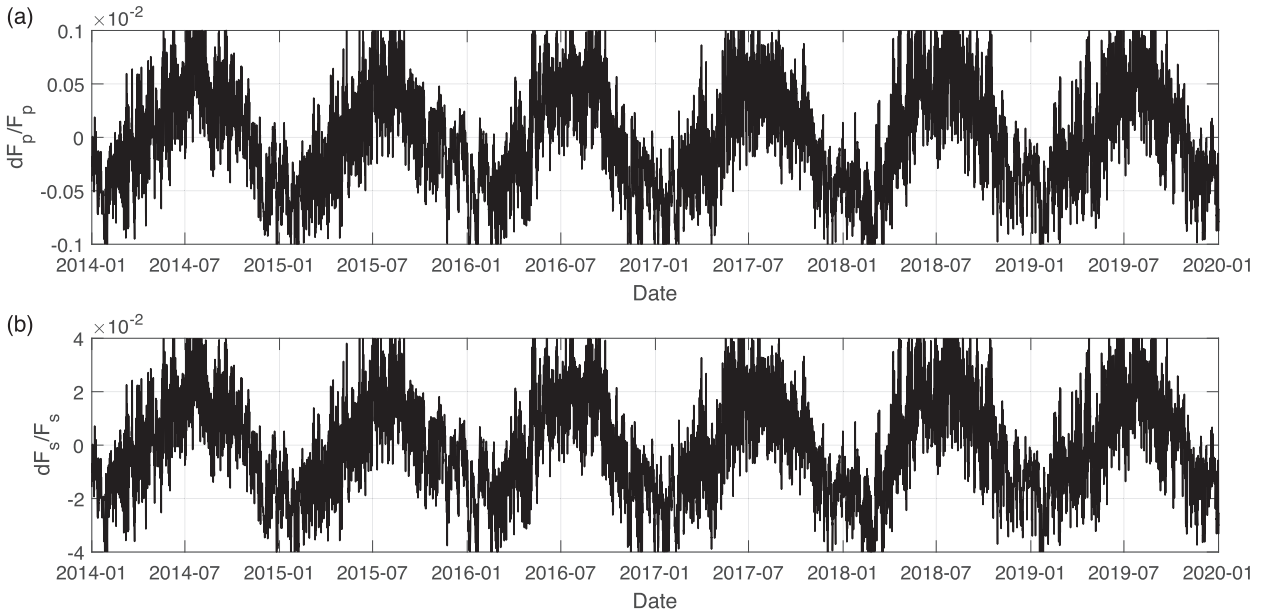


**Figure 7.** Relative change in site amplification due to the body-wave velocity variations modelled in Section 3.4 (Fig. 4).

experiments, temperature derivatives of the bulk modulus for saturated materials could potentially be approximated using the Gassmann equations, since Jaya *et al.* (2010) showed that fluid characteristics play a significant role in seismic wave speed changes in a laboratory setting, and the bulk modulus of water is a well-known parameter as a function of temperature. We could therefore use the Gassmann equations to compute the change in bulk modulus due to a substitution of water of a certain temperature with water of a different temperature, ultimately resulting in a temperature derivative of the bulk modulus. This discussion is a reminder that when using our approach for temperature monitoring, a detailed uncertainty analysis of the elastic constants is required. In our contribution, which is meant to identify how different mechanisms affect seismic wave speeds, it is less of a concern beyond being aware that uncertainties matter.

The modelled temperature evolution in Section 3.3 is also an approximation, since temperature changes due to advection and phase transitions (Rutten *et al.* 2010), and upward heat transport from the deep subsurface are not taken into account. Furthermore, not only are surface temperatures affected by air temperatures and radiation, air temperatures are also partly controlled by soil temperatures (e.g. Qin *et al.* 2023). Air temperature variations are therefore not a sole source for soil temperature changes, but merely an estimate of surface temperatures. Upward heat transport from the deep subsurface also results in a temperature gradient as shown by Ter Voorde *et al.* (2014). Such a steady gradient however does not affect the change in temperature, since only the second spatial derivative contributes to temporal changes (eq. 26). Phase transitions can also be a source for temperature change. As the contact area between liquid and gas is largest in the unsaturated subsurface, evaporation mostly affects the temperature in this layer. During the summer, this layer will slightly cool down due to evaporation, hence the temperature difference between summer and winter will be slightly smaller than presented in Fig. 2. This effect is rather small, as the modelled subsurface temperature differences between summer and winter are in the same order of magnitude as direct temperature measurements (Bense & Kooi 2004; Kole *et al.* 2020). Groundwater flow can also contribute to heat transport (Bense & Kooi 2004; de Louw *et al.*

2010). However, in the saturated subsurface, vertical flow is relatively low (maximum of  $360 \text{ mm yr}^{-1}$ , Kooi 2008), making heat transport through advection negligible compared to the yearly heat transport by diffusion. All these potential contributions to subsurface temperature changes do not pose a problem for our purpose, as we are mainly interested in the order of magnitude of daily and seasonal variations.

In Section 3.1, we made necessary assumptions regarding thermo-elastic changes, including the exclusion of vertical stress and horizontal strain, as well as an initial hydrostatic pressure for our region of interest. These assumptions are valid in a horizontally isotropic medium with no horizontal temperature variations and are reasonable in an unconsolidated setting as in the shallow subsurface of Groningen, where horizontal variations in geology are small, and vertical heat diffusion is the dominant mechanism for subsurface heat transport. These assumptions, however, need to be changed for different settings such as volcanoes, mountainous areas with a horizontally heterogeneous geology, or lake areas with large lateral temperature gradients.

Anelastic effects were not considered in our analysis. Due to a low shear strength there is a potential for reorganization in unconsolidated materials such as sand and clay, leading to the anelastic transmission of horizontal stress to vertical strain (Ben-Zion & Leary 1986). While the shear strength in unconsolidated materials is relatively small, it is not negligible (Liu *et al.* 2018). Therefore, shear stresses can indeed exist, but only when they exceed the shear strength will anelastic changes start to occur.

In our analysis, we did not consider temperature-induced changes in pore fluids. When the temperature rises under drained conditions, the pore fluid will expand as described by the thermal expansion coefficient of water ( $d\epsilon_{kk}^{\text{water}}/dT = 3\alpha_T^{\text{water}} = 2.2 \times 10^{-4} \text{ }^\circ\text{C}^{-1}$ ). Consequently, the corresponding body-wave velocity changes are smaller than the already insignificant blue curves in Figs 3(c) and (d) and can hence be neglected. The pore fluids therefore expand faster due to temperature changes ( $d\epsilon_{kk}^{\text{water}}/dT = 2.2 \times 10^{-4} \text{ }^\circ\text{C}^{-1}$ ) than the total volume including the pore space ( $d\epsilon_{kk}^{\text{total}}/dT = 0.6 \times 10^{-4} \text{ }^\circ\text{C}^{-1}$ ; Fig. 3b). This leads to groundwater migration, a slight increase of the groundwater level, and hence a

temperature-induced change in pore pressure and seismic velocity. It is however unknown how the porosity responds to expansion, hence we can only assess the order of magnitude for temperature-induced pore pressure change. The pore pressure  $u(z)$  is determined by the height  $h$  of the water column above depth  $z$ , the density of the pore fluid  $\rho_w$  and the gravitational acceleration  $g$  as  $u = h\rho_w g$ . For a relative increase of the water column of  $2.2 \times 10^{-4}$  of an initial  $h = 50$  m, the pore pressure increases by about  $du \sim 110$  Pa. These pore pressure effects are at least two orders of magnitude smaller than the pressure changes presented in Fig. 3(a), and can thus be neglected. Under undrained conditions, the restriction of pore fluid expansion however significantly affects the pore pressure and needs to be accounted for. We also did not consider the effect of freezing and thawing of the pore fluids on the elastic parameters either. Freezing of pore fluids significantly increases the shear modulus, consequently increasing body-wave velocities and decreasing site amplifications. This effect has not been taken into account. As Dutch winters are relatively mild (Fig. 2), the temperatures in the unsaturated subsurface rarely freezes. In colder environments this needs to be addressed though (e.g. James *et al.* 2019; Lindner *et al.* 2021).

We only considered surface-wave phase velocity changes through changes in shear wave speeds, and excluded density and compressional wave sensitivity kernels in eqs (12)–(14). We can justify this by two observations. Density and compressional wave sensitivity kernels are at least an order of magnitude smaller than shear wave sensitivity kernels, and temperature sensitivities of density and compressional wave velocity are at least one order of magnitude smaller than the temperature sensitivity of the shear wave velocity (Figs 3c and d).

The sensitivity kernels derived in our application establish a connection between temperature variations and surface-wave phase velocity changes. However, we should emphasize that a kernel-based approach is only valid for small perturbations. We believe that the velocity variations up to 8 per cent (Fig. 4) fall within the range of small perturbations.

In Section 3.5, we only considered changes in amplification due to temperature-induced body-wave speed changes at the surface, whereas in reality temperature variations affect body-wave speeds over a larger depth range. We further assumed a smooth impedance gradient. The errors introduced by these simplifications are much smaller than the values we find. We need to note however that temperature variations below well-insulated buildings may be smaller, leading to smaller amplifications, and the amplification factor at a building's foundation depth may be the more important factor for structure safety.

We focused on laterally homogeneous temperature variations. However, others considered lateral variations in temperature, leading to non-zero horizontal strains and vertical stresses (e.g. Berger 1975; Ben-Zion & Leary 1986; Ben-Zion & Allam 2013; Richter *et al.* 2014). Such configurations result in stresses and strains propagating much deeper than the actual temperature change, as illustrated in Tsai (2011, fig. 1). Consequently, body-wave speed changes are affected over greater depths, and surface wave phase velocity changes extend to lower frequencies. Ermert *et al.* (2023) discovered that low-frequency sensitivities to surface temperature variations are particularly prominent near lake zones, where significant lateral temperature gradients exist. For higher frequencies, they observed no distinction between zones with or without temperature gradients, suggesting that lateral temperature gradients do not significantly affect thermal stresses and strains in shallow layers. The approach presented here is mainly applicable at areas where large

water bodies are absent, otherwise lateral temperature gradients should be included.

Our analysis focused on the Groningen subsurface of the Netherlands, accommodating a thick layer of soft unconsolidated materials. Although the conclusions mostly apply to this specific region, the approach of Section 3 can be applied to any location where the theoretical framework of Section 2 holds. It simply requires a careful consideration on initial and boundary conditions as well as elastic parameters to establish the weight between the different effects.

We studied seismic wave speed changes resulting from natural daily and seasonal temperature variations at the surface, and our assumptions were tailored accordingly. However, in the context of subsurface heat-storage or geothermal power plants, certain assumptions need reconsideration. Specifically, we need to account for horizontal heat transport through diffusion and advection, as well as horizontal strain and vertical stress. Stricker *et al.* (2023) have demonstrated that it is possible to solve this problem semi-analytically (van Wees *et al.* 2019) for thermally induced stresses and strains, as well as for pore pressure changes resulting from injection and production. To evaluate the effect of thermo-elasticity on seismic velocities, we can still use eq. (5) in addition to appropriate initial and boundary conditions as well as elastic parameters.

Given the relationships between temperature, seismic velocities and site amplification, the question arises: does climate change pose a threat to human safety through changes in site amplification? The temperature sensitivities presented in Fig. 3(d) show that shear wave velocities decrease by 0.5 per cent per  $^{\circ}\text{C}$  at the surface, leading to an increase in site amplification of 0.25 per cent per  $^{\circ}\text{C}$ . Even when considering a pessimistic temperature scenario of  $dT = 4^{\circ}\text{C}$  by the year 2100 (fig. TS.4 in Pörtner *et al.* 2023), we predict an increase in site amplification in the order of only 1 per cent. Therefore, climate change has a minimal effect on site amplification.

## 5 CONCLUSIONS

We have investigated the effects of temperature on seismic properties in the shallow subsurface. For several end-member models, we computed the sensitivity of near-surface seismic properties to temperature variations. At a site in the Groningen region in the Netherlands, we estimated variations in subsurface temperature, evaluated thermally induced stresses and strains, and determined how these factors influence body-wave speeds, surface wave phase velocities, and site amplifications.

We have considered several mechanisms that contribute to velocity changes and found that the intrinsic temperature dependency of elastic moduli compete with thermally induced stresses in a thermo-elastic setting. In a purely elastic medium, pore pressure effects dominate. Our findings for the Groningen subsurface indicate that thermally induced dilatation is negligible and can hence be disregarded. The specific initial and boundary conditions, as well as the elastic parameters determine how the intrinsic temperature dependency of the elastic parameters and the thermally induced stresses are balanced. We suggest that this can potentially reconcile discrepancies observed between field and laboratory experiments. For Groningen, we note a distinct turning point at 6 m depth, above which the intrinsic temperature dependency dominates velocity changes, while below 6 m, thermal stress becomes the dominant factor.

Specifically for the shallow unconsolidated sediments in the subsurface of Groningen, where subsurface temperature fluctuations

are driven by seasonal atmospheric temperature fluctuations roughly between  $-5$  and  $30^{\circ}\text{C}$ , we predict seasonal temperature-induced changes in body-wave speeds up to 8 per cent in the first few metres of the subsurface, high-frequency (above 2 Hz) surface-wave phase velocity variations of approximately 1–2 per cent, and relative changes in site amplification in the order of 4 per cent. The competition between the two dominant mechanisms for velocity changes determines that site amplification is more enhanced during summer and decreased during winter.

## ACKNOWLEDGMENTS

This work is part of research programme DeepNL, financed by the Dutch Research Council (NWO) under project no. DeepNL.2018.033.

## DATA AVAILABILITY

This manuscript incorporated air temperature data of meteorological station 280 in Eelde, provided by the Royal Netherlands Meteorological Institute (KNMI 2023, <https://daggegevens.knmi.nl/klimatologie/uurgegevens>, last accessed: 2023 August 17). Models for shear and compressional-wave velocities, and density were retrieved from Ntinalexis *et al.* (2023) and Romijn (2017). These models are available through <https://osf.io/s3zxa/> (last accessed: 2023 September 6) and <https://nam-onderzoeksrapporten.data-app.nl/reports/download/groningen/en/3b4f8b0d-0277-40e0-8ff5-9a385c08327d> (last accessed: 2023 August 17), respectively.

## REFERENCES

- Bard, P.-Y., Campillo, M., Chavez-Garcia, F. & Sanchez-Sesma, F., 1988. The Mexico earthquake of September 19, 1985 – A theoretical investigation of large- and small-scale amplification effects in the Mexico City Valley, *Earthq. Spectra*, **4**(3), 609–633.
- Ben-Zion, Y. & Allam, A., 2013. Seasonal thermoelastic strain and post-seismic effects in Parkfield borehole dilatometers, *Earth planet. Sci. Lett.*, **379**, 120–126.
- Ben-Zion, Y. & Leary, P., 1986. Thermoelastic strain in a half-space covered by unconsolidated material, *Bull. seism. Soc. Am.*, **76**(5), 1447–1460.
- Bense, V. & Kooi, H., 2004. Temporal and spatial variations of shallow subsurface temperature as a record of lateral variations in groundwater flow, *J. geophys. Res.: Solid Earth*, **109**(B4), doi:10.1029/2003JB002782.
- Bentil, O.T. & Zhou, C., 2022. Effects of temperature and thermal cycles on the elastic shear modulus of saturated clay, *J. Geotech. Geoenviron. Eng.*, **148**(7), 06022006, doi:10.1061/(ASCE)GT.1943-5606.0002822.
- Berger, J., 1975. A note on thermoelastic strains and tilts, *J. geophys. Res.*, **80**(2), 274–277.
- Bièvre, G., Franz, M., Larose, E., Carrière, S., Jongmans, D. & Jaboyedoff, M., 2018. Influence of environmental parameters on the seismic velocity changes in a clayey mudflow (Pont-Bourquin Landslide, Switzerland), *Eng. Geol.*, **245**, 248–257.
- Birch, F., 1943. Elasticity of igneous rocks at high temperatures and pressures, *Bull. geol. Soc. Am.*, **54**(2), 263–286.
- Bobrowski, A., Drożyński, D., Jakubski, J., Szumera, M., Kaczmarek, K. & Grabowska, B., 2018. Thermal deformation of moulding and core sands with an inorganic binder containing a relaxation additive, *Arch. Foundry Eng.*, **18**, doi:10.24425/afe.2018.125175.
- Bommer, J.J., *et al.*, 2017. Framework for a ground-motion model for induced seismic hazard and risk analysis in the Groningen gas field, the Netherlands, *Earthq. Spectra*, **33**(2), 481–498.
- Bradley, B.A., 2012. Strong ground motion characteristics observed in the 4 September 2010 Darfield, New Zealand earthquake, *Soil Dynam. Earthq. Eng.*, **42**, 32–46.
- Christensen, N.I., 1979. Compressional wave velocities in rocks at high temperatures and pressures, critical thermal gradients, and crustal low-velocity zones, *J. geophys. Res.: Solid Earth*, **84**(B12), 6849–6857.
- Colombero, C., Baillet, L., Comina, C., Jongmans, D., Larose, E., Valentin, J. & Vinciguerra, S., 2018. Integration of ambient seismic noise monitoring, displacement and meteorological measurements to infer the temperature-controlled long-term evolution of a complex prone-to-fall cliff, *J. geophys. Int.*, **213**(3), 1876–1897.
- Dandekar, D.P. & Ruoff, A.L., 1968. Temperature dependence of the elastic constants of calcite between 160 and 300 K, *J. appl. Phys.*, **39**(13), 6004–6009.
- de Louw, P.G., Essink, G.O., Stuyfzand, P.J. & van der Zee, S., 2010. Upward groundwater flow in boils as the dominant mechanism of salinization in deep polders, the Netherlands, *J. Hydrol.*, **394**(3–4), 494–506.
- Ermert, L.A., Cabral-Cano, E., Chaussard, E., Solano-Rojas, D., Quintanar, L., Morales Padilla, D., Fernández-Torres, E.A. & Denolle, M.A., 2023. Probing environmental and tectonic changes underneath Mexico City with the urban seismic field, *Solid Earth*, **14**(5), 529–549.
- Fokker, E., Ruigrok, E., Hawkins, R. & Trampert, J., 2021. Physics-based relationship for pore pressure and vertical stress monitoring using seismic velocity variations, *Remote Sens.*, **13**(14), 2684, doi:10.3390/rs13142684.
- Fokker, E., Ruigrok, E., Hawkins, R. & Trampert, J., 2023. 4D physics-based pore pressure monitoring using passive image interferometry, *Geophys. Res. Lett.*, **50**(5), e2022GL101254, doi: 10.1029/2022GL101254.
- Hawkins, R., 2018. A spectral element method for surface wave dispersion and adjoints, *J. geophys. Int.*, **215**(1), 267–302.
- James, S., Knox, H., Abbott, R., Panning, M. & Scream, E., 2019. Insights into permafrost and seasonal active-layer dynamics from ambient seismic noise monitoring, *J. geophys. Res.: Earth Surface*, **124**(7), 1798–1816.
- Jaya, M.S., Shapiro, S.A., Kristinsdóttir, L.H., Bruhn, D., Milsch, H. & Spangenberg, E., 2010. Temperature dependence of seismic properties in geothermal rocks at reservoir conditions, *Geothermics*, **39**(1), 115–123.
- Kern, H., 1978. The effect of high temperature and high confining pressure on compressional wave velocities in quartz-bearing and quartz-free igneous and metamorphic rocks, *Tectonophysics*, **44**(1–4), 185–203.
- KNMI, 1993. *Netherlands Seismic and Acoustic Network*, Royal Netherlands Meteorological Institute (KNMI), Other/Seismic Network.
- KNMI, 2023. *Climatology: Hourly Observations of the Weather in the Netherlands*, Royal Netherlands Meteorological Institute (KNMI), <https://daggegevens.knmi.nl/klimatologie/uurgegevens> (Last accessed 2024 March 22).
- Kohnen, H., 1974. The temperature dependence of seismic waves in ice, *J. Glaciol.*, **13**(67), 144–147.
- Kole, P., Cannon, M., Tomic, J. & Bierman, S., 2020. *Analysis of and learnings from the first four years of in-situ strain data in Zeerijp-3A*, Tech. rep., Nederlandse Aardolie Maatschappij NV, Assen, the Netherlands.
- Kooi, H., 2008. Spatial variability in subsurface warming over the last three decades; insight from repeated borehole temperature measurements in the Netherlands, *Earth planet. Sci. Lett.*, **270**(1–2), 86–94.
- Kruiver, P.P. *et al.*, 2017. Characterisation of the Groningen subsurface for seismic hazard and risk modelling, Netherlands, *J. Geosci.*, **96**(5), s215–s233.
- Lakshatanov, D.L., Sinogeikin, S.V. & Bass, J.D., 2007. High-temperature phase transitions and elasticity of silica polymorphs, *Phys. Chem. Mineral*, **34**, 11–22.
- Lecocq, T., Longuevergne, L., Pedersen, H.A., Brenguier, F. & Stammer, K., 2017. Monitoring ground water storage at mesoscale using seismic noise: 30 years of continuous observation and thermo-elastic and hydrological modeling, *Sci. Rep.*, **7**(1), 1–16.
- Lindner, F., Wassermann, J. & Igel, H., 2021. Seasonal freeze-thaw cycles and permafrost degradation on Mt. Zugspitze (German/Austrian Alps) revealed by single-station seismic monitoring, *Geophys. Res. Lett.*, **48**(18), e2021GL094659, doi:10.1029/2021GL094659.



- Liu, H., Liu, H., Xiao, Y. & McCartney, J.S., 2018. Effects of temperature on the shear strength of saturated sand, *Soils Found.*, **58**(6), 1326–1338.
- Mandelis, A., 2001. *Diffusion-wave Fields: Mathematical Methods and Green Functions*, Springer Science & Business Media.
- McKinstry, H.A., 1965. Thermal expansion of clay minerals, *Amer. Mineral.*, **50**(1–2), 212–222.
- Ntinalexis, M. *et al.*, 2023. A database of ground motion recordings, site profiles, and amplification factors from the Groningen gas field in the Netherlands, *Earthq. Spectra*, **39**(1), 687–701.
- Ohno, I., 1995. Temperature variation of elastic properties of  $\alpha$ -quartz up to the  $\alpha$ - $\beta$  transition, *J. Phys. Earth*, **43**(2), 157–169.
- Orlander, T., Andreassen, K.A. & Fabricius, I.L., 2021. Effect of temperature on stiffness of sandstones from the deep North Sea basin, *Rock Mech. Rock Eng.*, **54**(1), 255–288.
- Pham, Q.T., 1985. A fast, unconditionally stable finite-difference scheme for heat conduction with phase change, *Int. J. Heat Mass Transf.*, **28**(11), 2079–2084.
- Pörtner, H.-O. *et al.*, 2023. IPCC: technical summary, in *Climate Change 2022: Impacts, Adaptation and Vulnerability*. Cambridge University Press, Cambridge, UK and New York, USA. pp. 37–118.
- Qin, L., Qiu, H., Nakata, N., Deng, S., Levander, A. & Ben-Zion, Y., 2023. Variable daily autocorrelation functions of high-frequency seismic data on mars, *Seismol. Soc. Am.*, **94**(2A), 746–758.
- Radkovský, F. *et al.*, 2022. Effect of the composition of hybrid sands on the change in thermal expansion, *Materials*, **15**(17), 6180, doi:10.3390/ma15176180.
- Richter, T., Sens-Schönfelder, C., Kind, R. & Asch, G., 2014. Comprehensive observation and modeling of earthquake and temperature-related seismic velocity changes in northern Chile with passive image interferometry, *J. geophys. Res.: Solid Earth*, **119**(6), 4747–4765.
- Rodriguez-Marek, A., Kruiver, P.P., Meijers, P., Bommer, J.J., Dost, B., van Elk, J. & Doornhof, D., 2017. A regional site-response model for the Groningen gas field, *Bull. seism. Soc. Am.*, **107**(5), 2067–2077.
- Romijn, R., 2017. *Groningen velocity model 2017*, Tech. rep., Nederlandse Aardolie Maatschappij NV, Assen, the Netherlands.
- Ruigrok, E., Rodriguez-Marek, A., Edwards, B., Kruiver, P., Dost, B. & Bommer, J., 2022. Derivation of a near-surface damping model for the Groningen gas field, *J. geophys. Int.*, **230**(2), 776–795.
- Rutten, M.M., Steele-Dunne, S.C., Judge, J. & van de Giesen, N., 2010. Understanding heat transfer in the shallow subsurface using temperature observations, *Vadose Zone J.*, **9**(4), 1034–1045.
- Sens-Schönfelder, C. & Wegler, U., 2006. Passive image interferometry and seasonal variations of seismic velocities at Merapi Volcano, Indonesia, *Geophys. Res. Lett.*, **33**(21), doi:10.1029/2006GL027797.
- Sleeman, R. & de Zeeuw-van Dalfsen, E., 2020. Cross-correlation analysis of long-term ambient seismic-noise recordings in the Caribbean Netherlands to monitor the volcanoes on Saba and St. Eustatius, *Bull. seism. Soc. Am.*, **110**(5), 2541–2558.
- Stricker, K., Egert, R., Fokker, P., Vardon, P.J., van Wees, J.D., Schill, E. & Kohl, T., 2023. Risk assessment of high-temperature heat storage (HT-ATES) at the DeepStor demonstrator site, in *EGU General Assembly*, Vol. **2023**.
- Svidró, J., Diószegi, A. & Svidró, J.T., 2020. The origin of thermal expansion differences in various size fractions of silica sand, *Int. J. Cast Metals Res.*, **33**(6), 242–249.
- Ter Voorde, M., van Balen, R., Luijendijk, E. & Kooi, H., 2014. Weichselian and Holocene climate history reflected in temperatures in the upper crust of the Netherlands, *J. Geosci.*, **93**(3), 107–117.
- Tromp, J. & Trampert, J., 2018. Effects of induced stress on seismic forward modelling and inversion, *J. geophys. Int.*, **213**(2), 851–867.
- Tsai, V.C., 2011. A model for seasonal changes in GPS positions and seismic wave speeds due to thermoelastic and hydrologic variations, *J. geophys. Res.: Solid Earth*, **116**(B4), doi:10.1029/2010JB008156.
- van Ginkel, J., Ruigrok, E. & Herber, R., 2019. Assessing soil amplifications in Groningen, the Netherlands, *First Break*, **37**(10), 33–38.
- van Wees, J.-D. *et al.*, 2019. 3-D mechanical analysis of complex reservoirs: a novel mesh-free approach, *J. geophys. Int.*, **219**(2), 1118–1130.